Effect of the electrical discharge machining on Ti6Al4V corrosion behaviour in simulated body fluid

J.I. Ahuir-Torres[1], H.R. Kotadia[2] and T.T. Öpöz[1]

[1]General Engineering Research Institute, School of Engineering, Faculty of Engineering and Technology, Liverpool John Moores University, Byrom Street, Liverpool, L3 3AF, United Kingdom.

[2] School of Engineering, Faculty of Engineering and Technology, Liverpool John Moores University, Byrom Street, Liverpool, L3 3AF, United Kingdom.

Corresponding Author´s email: j.i.ahuirtorres@ljmu.ac.uk

Abstract

Titanium alloys, such as Ti6Al4V, are widely employed in the biomedical industry for implant applications due to their favourable properties. However, these alloys can experience long-term corrosion in the presence of bodily fluids, which is a critical concern for implants as it affects their timespan. Therefore, this study aimed to examine the corrosion resistance of Ti6Al4V in body fluid. Highly desirable electrical discharge machining (EDM) techniques used for Ti6Al4V sample preparation with three different conditions (oil, deionized water, and hydroxyapatite mixed in deionized water). Corrosion was assessed using electrochemical analyses, with microstructural analysis. Results indicated that the samples produced using water and oil had the best and lowest corrosion resistance, respectively. Protective oxide layer formed during the EDM in water while heterogeneous surface was produced for EDM in oil. The increase in capacitance leads to the thickening of the oxide layer, thereby enhancing the corrosion resistance.

Keywords: Ti6Al4V; Electrical Discharge Machining; Corrosion; Electrochemical Analyses.

1. Introduction

Titanium alloys, specifically Ti6Al4V, are widely employed as implant for the biomedical industry owing to the excellent properties as good corrosion resistance and excellent biointegrity [1-5].The increasing life expectancy has, nevertheless, necessitated the need to extend the lifespan of implants to span several decades. The aggressive environment of the body fluid can corrode the Ti6Al4V at long-term. This can decrease the biointegrity and lifetime of this metallic material and produce the loosing of the implant after long-term [1, 4, 6]. The titanium dental implant can be corroded in saliva environment due to fluorine ions. Ti6Al4V passive film can be dissolved in the environment via the reaction of the fluorine ions that is highly chemical affinity to the titanium [5, 7]. Chlorine, sulphate and phosphate ions of the blood can also react the passive film of Ti6AlV, causing the breaking down the film and beginning the corrosion the implant [4, 6, 8]. The breaking of the passive film is furthermore encouraged by the body temperature (37.5° C). The increase of the temperature accelerates the ion reactions with the passive film [4, 9]. In addition to the loss of the implant, the corrosion of Ti6Al4V can provoke other health problems because of the alloying elements. Aluminium is associated to the Alzheimer while vanadium is cytotoxic [3, 10]. Thus, the increment of the corrosion resistance is an essential to improve the Ti6Al4V capacities as implants.

The corrosion resistance of the titanium alloy can be improved using varying techniques including, anodising [11, 12], plasma electrolytic oxidation [13], electrical discharge machining (EDM) [1, 14-17], ion implantation [18], sol-gel coatings [19], laser alloying [2], laser selective melting [20], thermal treatment [8], physical vapour deposition [21] and chemical vapour deposition [22]. EDM enhanced the corrosion resistance of the Ti alloy by generating layers with high chemical inactivity and good adhesion on the subtract [1]. The characteristics of the layers are dependent on the specific EDM conditions and type of the bath used. In non-aggressive environments, EDM induces microstructural changes in the titanium alloy, resulting in the formation of a new layer with high corrosion resistance [17]. When EDM is performed in a water bath, a thick passive film is produced on the metallic alloy, thereby increasing its corrosion resistance [16]. In the case of the EDM in hydroxyapatite dissolution bath, in addition to the thick passive film, a hydroxyapatite layer can be generated on the substrate through particle electrical deposition. This deposited layer exhibits excellent compaction and adhesion, providing protection for the metallic alloy against aggressive environments [1, 15]. Although similar effects were found in machined alloys with bath with carbon nanotubes [2], the hydroxyapatite layer possesses the benefit of increasing the material biocompatibility [14]. However, it is important to note that despite the corrosion resistance improvement achieved through EDM on Ti6Al4V, the process can also introduce cracks and pores. These imperfections can increase the titanium alloy's susceptibility to corrosion [23, 24]. The occurrence of these imperfections is influenced by the specific EDM conditions, such as capacitance and bath type [25, 26].

EDM technique furthermore is one of most suitable techniques to machine high strength and low thermal conductive materials. EDM is a non-contact machining method that utilizes a series of controlled electrical sparks between the workpiece and an electrode to erode the material. EDM offers several advantages for Ti alloy machining, including the ability to achieve intricate shapes, precise tolerances, and excellent surface finishes.

Additionally, EDM is a relatively low-temperature process, which helps to minimize the risk of thermal damage or distortion to the titanium alloy workpiece. In the context of bioimplant applications, the EDM technique enhances biocompatibility and promotes the desired surface roughness, facilitating improved wettability, hydrophilicity (allowing bone cells to adhere to the surface), proliferation, and anchorage [27-32].

The influence of EDM conditions on the corrosion resistance of machined Ti6Al4V in body fluid has been inadequately examined in the existing literature. Therefore, this study aims to investigate the corrosion resistance of Ti6Al4V machined through EDM under varying capacitance and bath conditions in simulated body fluid (SBF). The machining process was conducted using capacitances of 10nF, 100nF, and 500nF, and baths consisting of oil, water, and hydroxyapatite dissolution (HA). The surfaces and cross-sections of the samples were analysed using optical light profilometry and scanning electron microscopy, while the chemical composition was assessed using energy dispersive spectroscopy. The corrosion resistance and corrosion mechanism were evaluated through various electrochemical corrosion analyses, including potentiodynamic polarization curves (PPC) and electrochemical impedance spectroscopy (EIS) before and after the PPC test.

2. Experimental Setup

2.1. Materials and Electrical Discharge Machining

In this study, a Ti-6 wt.% Al-4 wt.% V alloy was used as the workpiece material in the form of a 3 mm thick sheet. The sheet was cut into a small rectangular piece measuring 55x80 mm. The experiments were conducted using a Hurco 50A Mark 2 die sinking type EDM machine.

For the electrode material, a solid circular graphite with a diameter of 6 mm was employed. To perform the EDM experiments under different dielectric conditions, a small dielectric reservoir was utilised, and the dielectric circulation system of the EDM machine was disconnected. The experimental setup is shown in **Fig. 1**.

Three different dielectric fluid conditions were employed in the experiment: EDM oil, deionized water, and a HA in deionized water. Hydroxyapatite powder, provided by Medicoat SAS based in France, with particle sizes ranging from 10 to 15 µm was mixed with deionized water at a concentration of 10 g/L. A digital mixer was used to stir the dielectric fluid, preventing precipitation of hydroxyapatite powder and accumulation of debris and HA particles in the machining zone.

The EDM machine's capacitance was set at three different values: 10nF, 100nF, and 500nF. A summary of the experimental parameters is presented in **Table 1**. **Fig. 2** illustrates the surfaces generated using EDM, consisting of 27 circular surfaces created under various dielectric fluid and capacitance settings. Each test was repeated three times to ensure the repeatability of the experiments.

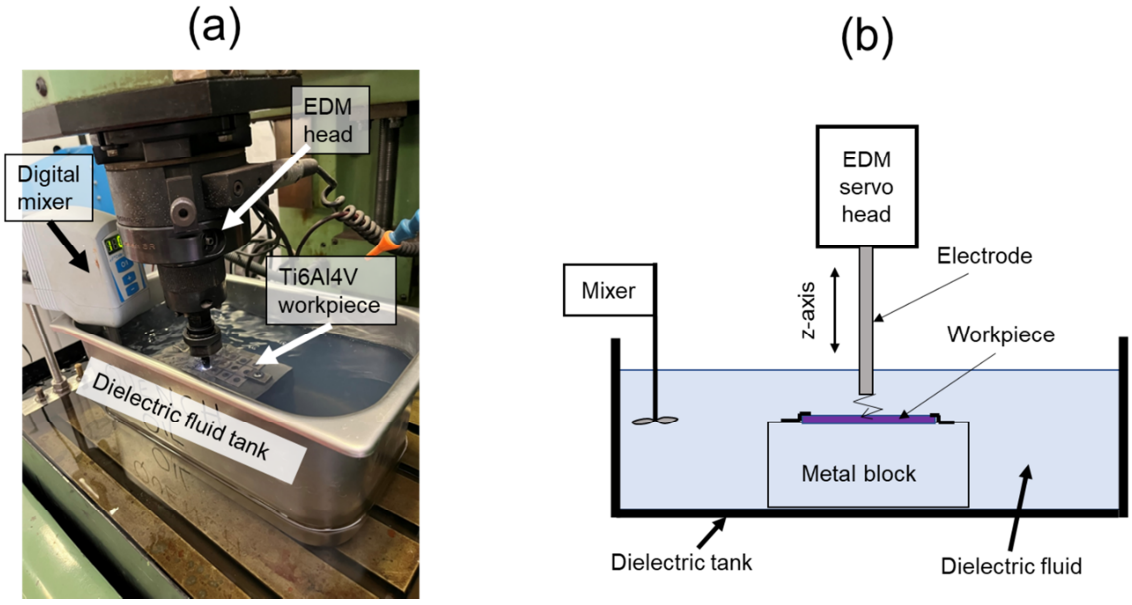

Figure 1. EDM machining setup (a) EDM set-up, (b) a schematic drawing of the experimental setup.

Table 1. Summary of EDM parameters used for the experiments.

Parameter	Description/Values
EDM machine	Hurco 50A Mark 2
Workpiece material	Ti6Al4V
Electrode	Solid circular graphite (6 mm in dia.)
Dielectric fluid	• Fully Synthetic Dielectric Oil (Corsmot EDM/CH PLUS) • Deionised water, • HA mixed in deionised water (10g/L HA concentration)
Pulse time (µs)	20
Duty cycle (%)	50
Capacitance (nF)	10, 100, 500
Polarity (electrode)	Negative

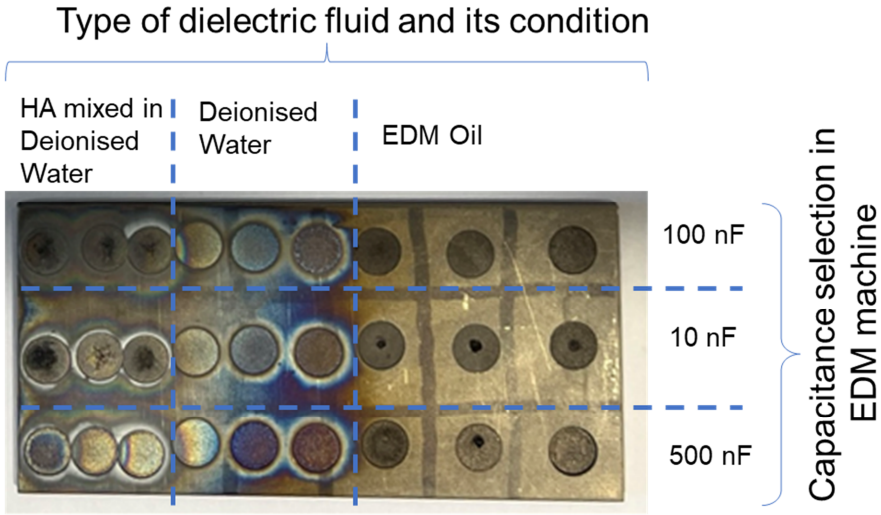

Figure 2. Macrostructures of EDMed Ti6Al4V workpiece material under different conditions.

2.2. Electrochemical Analyses

The non-electrical discharge machined (non-EDMed) samples also were polished with 1200p silicon carbide abrasive paper. All samples were cleaned after electrochemical analyses with commercial detergent and fresh water soaking, then with distilled water rinsing and the last cleaning step was isopropanol spray and drying with drier. The aggressive environment was SBF formed of the next chemical compounds summarised in **Table 2** [6, 12, 33].

Table 2. SBF chemical compounds in g/L [6, 12, 33].

Chemical compound	Quantity (g per litre distilled water)
NaCl	8.035
$NaHCO_3$	0.355
KCl	0.225
$K_2HPO_4.3H_2O$	0.231
$MgCl_2.H_2O$	0.311
$CaCl_2.H_2O$	0.292
Na_2SO_4	0.072
$((CH_2OH)_3(CNH_2)$	6.118
pH	7.4

The chemical products used were provided by Merck. The pH of the SBF environment was adjusted using 1 M HCl, and the pH measurements were taken using a pH meter (Jenway 350pH Meter) supplied by Scientific Laboratory Supplies. The temperature of the SBF was maintained at 315.5 K throughout the testing, achieved using a hot plate (Stuart, SB162) provided by BioCote.

The electrochemical experiments were conducted using a potentio/galvanostat (Interface1010E) from Gamry Instruments Inc. The potentio/galvanostat was handled with *Gamry Framework* software and the data were evaluated by mean of the *Gamry Echem Analyst* software. The three-electrode cell was employed to carry out the electrochemical analyses. The cell was consisted of a reference, counter and working electrode. The reference electrode was silver/silver chloride in 3 M KCl (Ag/AgCl 3 M KCl) with double junction, being supplied by EDT direct ion limited. The counter electrode was a platinum wire of 0.7 mm diameter that was provided by Cooksonglod Heimerle + Meule Group. The working electrodes were the samples. The electrochemical testing was perturbative of direct current (PPC) and of alternating current (EIS). PPC and EIS specifications were summarised in **Table 3.**

Table 3. Selected PPC specifications and EIS set up parameters.

Technique	Parameter	Value
PPC	Open circuit potential time	15 min
	Initial potential	Open circuit potential – 0.3 V
	Final potential	2.0 V vs Ag/AgCl 3M KCl
	Potential rate	0.167 mV/s
EIS	Potential amplitude in root mean square	10 mV
	Frequency range	Form 0.01 Hz to 100000 Hz
	Number of point per frequency decade	10

The samples were analysed with the next sequence of the techniques: EIS, PPC and EIS. The first EIS was made to study the corrosion mechanism of the non-polarised samples whilst the second EIS was conducted to understand the corrosion process of the samples polarised with PPC. The equivalent circuit method was utilised to assess the EIS data. *Gamry Echem Analyst* software was employed to develop the equivalent circuit method. All individual tests were repeated a minimum of three times to ensure the accuracy and reliability of the data.

2.3. Surface and Microstructure Analysis Methods

The EDM surfaces were analysed before and after the corrosion process using various microscopy techniques. Surface topography and roughness analyses of the EDM surfaces were performed using a Bruker Contour GT-K 3D white light interferometer equipped with *Vision 64* software (Optical light profilometer). The average areal surface roughness (Sa) values were used to compare the surface roughness of EDM surfaces under different dielectric fluid conditions and capacitance settings.

The surface characteristics and chemical composition of the samples were analysed using Scanning Electron Microscopy (SEM) with Energy Dispersive Spectroscopy (EDS). The SEM analysis was conducted at 10 kV with an 8.0 nA current and a 2.0 spot size. To prepare the samples for SEM analysis, standard Buehler grinding methodology was employed, followed by polishing using up to 0.05 µm. After polishing, the samples were subjected to a 2-hour treatment with VibroMet^{TM} using a silica suspension liquid.

3. Results

3.1. Surface and Microstructure Analyses after EDM

Fig. 3 illustrates the experimental results of surface roughness for different capacitance values (10nF, 100nF, and 500nF) and dielectric conditions (EDM oil, deionized water, and HA in deionized water). The surfaces machined in EDM oil exhibited higher surface roughness compared to those machined in deionized water, regardless of the capacitance values. The surface roughness values demonstrated an increasing trend with the rise in capacitance from 10nF to 500nF, for both dielectric fluids, EDM oil, and water. The heightened capacitance led to an elevation in the heat energy produced per spark in the EDM system, resulting in the creation of larger craters on the surface of the workpiece. This effect was particularly significant due to the occurrence of multiple sparks throughout the EDM erosion process. It was not possible to observe individual crater formation due to a single spark. Consequently, numerous craters were formed on the machined surface, contributing to the roughness of the EDMed surfaces. The surface roughness of the surfaces machined in HA mixed in deionized water did not exhibit a consistent increasing or decreasing trend with varying capacitance values. Among the different capacitance values, the surfaces machined with a capacitance of 10nF and HA mixed deionized water showed the highest surface roughness values. This can be attributed, in part, to the presence of HA powder causing unstable discharging and the low discharge energy not generating a strong pumping effect to remove debris particles in the discharging zone. The accumulation of debris particles and HA powder disrupted the discharging mechanism, resulting in higher surface roughness with a high standard deviation

of 1.094 at 10nF capacitance. In contrast, the standard deviations of surface roughness obtained with EDM oil and deionized water at 10nF capacitance were 0.191 and 0.126, respectively, indicating more stable and repeatable results.

Higher capacitance values allowed the discharge mechanism to generate greater heat energy and stronger sparks, resulting in an adequate pumping effect that effectively expelled debris particles and HA powder from the machining region. This led to a more stable and predictable process. The standard deviations of surface roughness for the surfaces machined in HA mixed deionized water with capacitance values of 100 nF and 500 nF were 0.194 and 0.290, respectively, indicating improved repeatability compared to the surfaces machined with a lower capacitance of 10nF. When considering larger capacitance values, such as 100nF and 500nF, EDM with HA mixed deionized water demonstrated superior surface roughness compared to surfaces machined with EDM oil and water. This improved surface roughness can be attributed to the alteration of the discharge mechanism due to the inclusion of powder. The mechanism of powder mixed EDM has been extensively discussed in the literature [27], where smaller and more frequent discharges are generated in powder EDM. This leads to the formation of smaller craters with each discharge, ultimately resulting in reduced surface roughness compared to non-powder EDM processes.

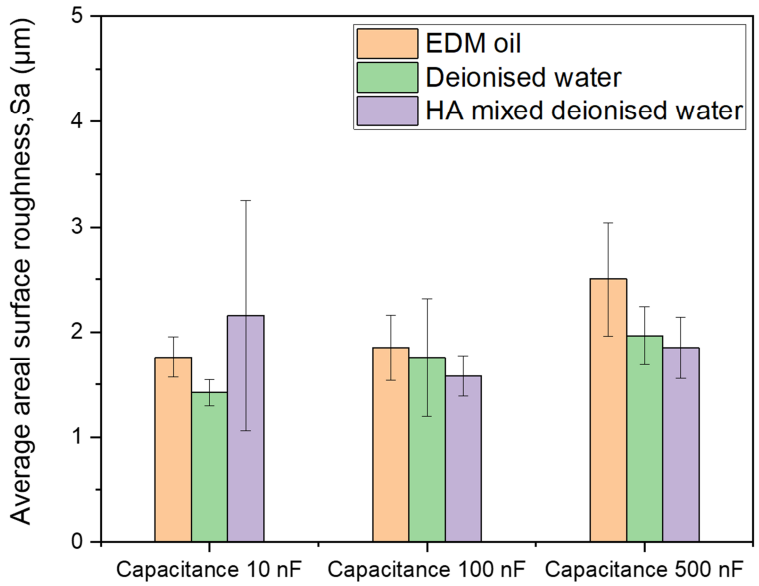

Figure 3. Average areal surface roughness (*Sa*) of the EDMed surfaces.

Fig. 4 presents a supporting 3D surface topography obtained from the Bruker interferometer, where the red colour indicates the distribution of heights from the valley. As depicted in **Fig. 4**, the surfaces machined via EDM in oil and deionized water exhibit a significant increase in roughness as the capacitance values are raised. Additionally, the surfaces machined in EDM oil tend to have rougher surfaces compared to other surfaces except the surfaces machined with HA mixed deionized water with 10nF setting. However, surfaces machined with HA mixed deionized water demonstrate improved surface finish compared to both EDM oil and deionized water, except when the capacitance value was set to 10nF.

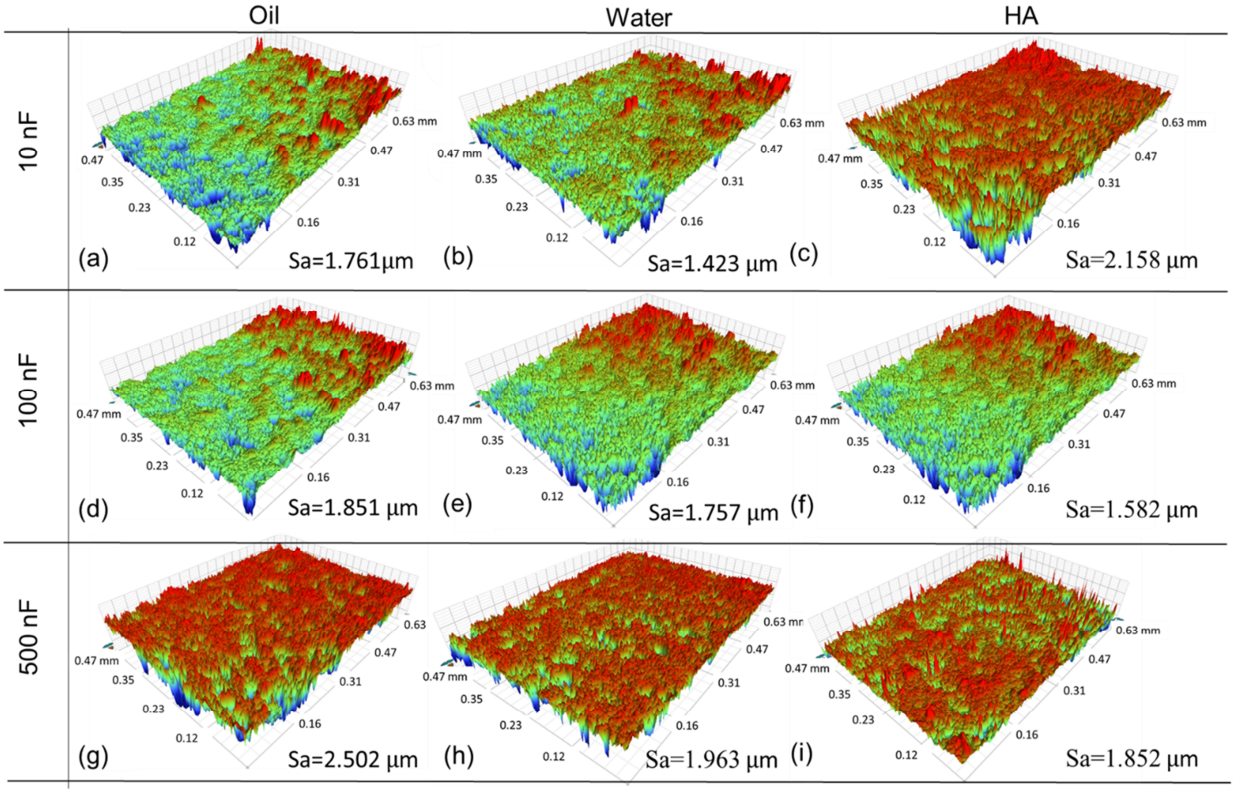

Figure 4. Bruker 3D surface topography images of electric discharge machined (EDMed) surfaces at different capacitance levels: (a-c) 10nF, (d-f) 100nF, and (g-i) 500nF. The images show the surfaces before corrosion in (a), (d), and (g) oils, (b), (e), and (h) distilled water, and (c), (f), and (i) a bath containing a mixture of hydroxyapatite and distilled water.

Fig. 5 illustrates the SEM images of cross-sectional view of EDMed samples. Typically, cross-sectional analysis is conducted in EDM-related research to examine the characteristics of the white layer (molten layer) including hardness, crack formation, heat-affected zone, and its thickness. However, in this study, the focus is on identifying characteristics such as cracks or different layer formations that might affect the corrosion analysis. The resolidified layer (white layer) becomes thicker as the capacitance value increases, which is directly related to the amount of energy applied to the surfaces. EDM mechanisms with higher capacitance values generate more significant heat energy, resulting in a thicker resolidified layer. While electrical discharge machining with EDM oil does not produce many cracks on the sub-surfaces, machining with deionized water and HA mixed deionized water leads to the formation of several cracks on the resolidified layer. The cracks formed with deionized water alone are larger and more prominent compared to the cracks formed with HA mixed deionized water. The oil EDM sample exhibits voids and holes on the machined area. The impacts of these characteristics on the corrosion analysis will be discussed in the subsequent section.

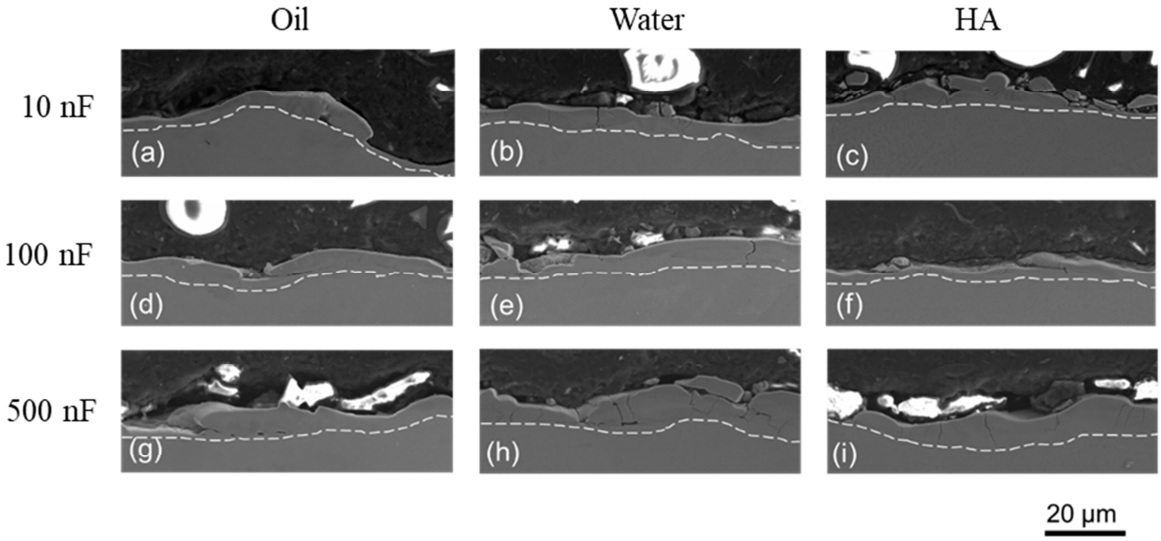

Figure 5. SEM images of cross-sectional view of non-corroded EDMed surfaces at (a-c) 10nF, (d-f) 100nF and (g-i) 500nF in (a), (d) and (g) oil, (b), (e) and (h) deionised water (water) and (c), (f) and (i) HA mixed with distilled bath (HA), where the dotted white line indicates the presence of the white layer (molten layer).

3.2. Electrochemical Assessments

3.2.1. Potentiodynamic Polarisation Curves, Direct Current.

All samples were subjected to testing using SBF to generate the potentiodynamic polarization curve. **Fig. 6** illustrates the resulting PPC curve obtained from all samples. As shown in **Fig. 6**, the potentiodynamic polarization curves exhibited a similar shape.

The reduction or cathodic branch of the curve appeared as a horizontal line, indicating that the cathodic reaction is primarily controlled by activation [34]. On the other hand, the anodic or oxidation branch of the curve displayed a vertical shape at low potential, indicating the presence of a passive film on the samples [12, 34]. At high potential, the curve exhibited a slight incline, indicating the occurrence of transpassivation of titanium dioxide (TiO_2 [12]) which transforms into other oxide forms such as TiO_4 or non-stoichiometric oxides. These oxidised forms also possess a protective/passive nature [5, 35, 36] as indicated by the vertical shape of the curve at the highest potential. The potential at which the transition from passivation to transpassivation occurs is often referred to as the transpassivation potential (E_{tp}) [35]. Some samples (EDMed samples at 100nF and 500nF in water and HA bath) exhibited current fluctuations in the cathodic branch, indicating the generation of metastable micropitting [35, 36].

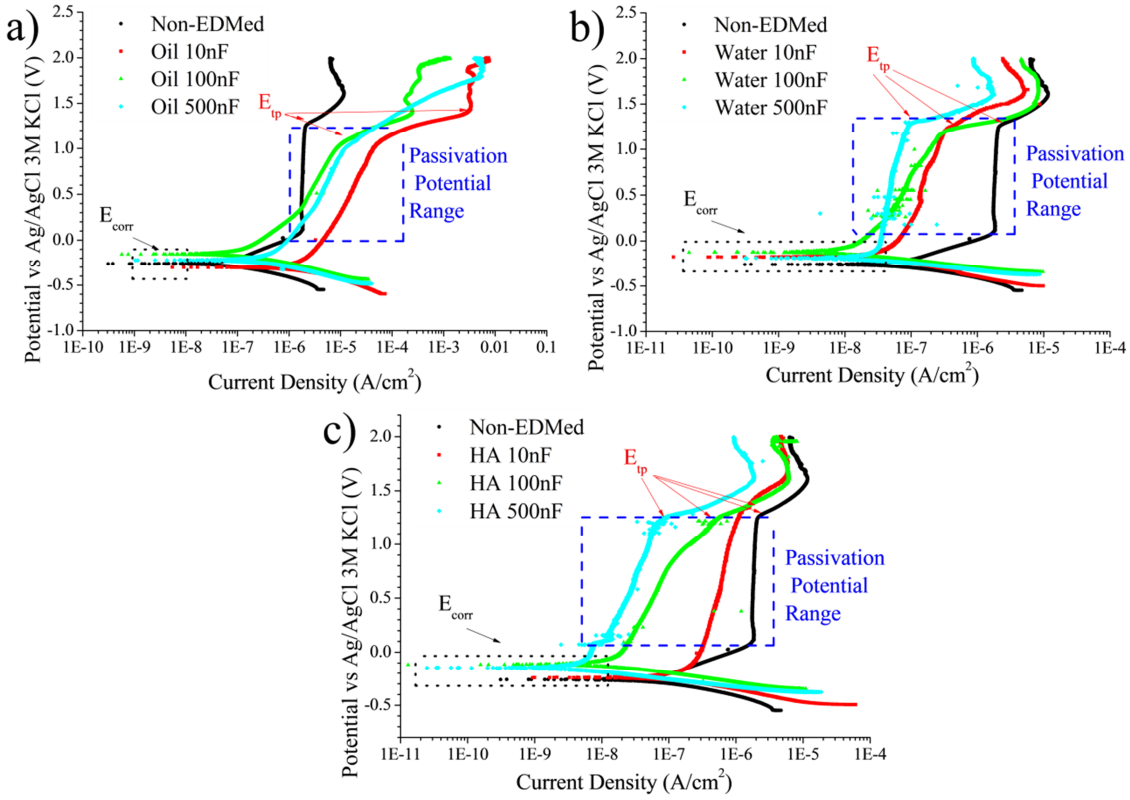

Figure 6. PPC of non-machined (non-EDMed) and electrical discharge machined Ti6Al4V at 10 nF, 100 nF and 500 nF with (a) oil, (b) distilled water (water) and (c) hydroxyapatite dissolution (HA) in SBF immersion at 7.4 pH and 313 K.

The corrosion characteristics of the samples, such as corrosion potential, corrosion rate, passivation potential range and passivation rate, polarization resistance, and transpassivation potential, varied among the different samples (**Fig. 7**). These features were determined based on the data obtained from the PPC. The majority of the machined samples had higher corrosion potential (E_{corr}) than that for non-EDMed samples (**Fig. 7(a)**). The oxidised layer generated during EDM is nobler than native passive film. The electrical discharges activate the metal to react with the aggressive environment, producing a compact oxidised layer [15]. The only exception was the samples machined at 10nF and oil bath where E_{corr} was lower than non-EDMed samples. The low capacitance and aggressiveness of the environment hinder the completed oxidised layer formation. The imperfections as cracks, cavities and inhomogeneity can also decrease the nobility of the metallic materials [37]. E_{corr} of the samples produced in more aggressive environment (water and hydroxyapatite dissolution) was higher than less harsh environment (oil bath). The oxidative environment produces oxidised layer thicker than the layers created in less harsh bath. The nobility of the oxide layer is proportional to the thickness and homogeneity [38]. In respect of the capacitance, EDMed Ti6Al4V samples created at 100nF had higher E_{corr} for water and HA baths. The thickness and homogeneity of the oxide layer also is proportional to capacitance [1]. An excessive capacitance can produce imperfections (e.g., cracks and pores) and other oxidised forms that diminishes the nobility of the alloy [2, 23].

The corrosion rate ($C.R._{corr}$) of the samples can be observed in **Fig.7(b)** and these were estimated using equation (1) [2, 16, 39, 40].

$$C.R._{corr} = \frac{I_{corr} * M}{\rho * F * n} \quad (1)$$

Where, I_{corr} is the corrosion current density, M is the titanium molar mass (47.867 g/mol [41]), ρ is the Ti6Al4V density (4.43 g/cm^3 [42]), F is the Faraday´s constant (96500 coulombs per mole (C/mol) [43]) and n is the electron number transferred in the corrosion reaction (4 electrons [41]). I_{corr} was estimated with the intersection of the cathodic and anodic Tafel linear regression [3, 44]. The choice of this particular corrosion feature was based on its ability to provide a more visually tangible representation of the corrosion kinetics. The majority of the machined samples had lower $C.R._{corr}$ than non-machined samples. The oxidised layer formed during EDM is compact and protective, being a passive film [36, 40]. The chemical inactivity of the passive film commonly is proportional to its thickness [1]. Note that the samples machined in hydroxyapatite dissolution bath, the deposition of the hydroxyapatite on surface can create an extra protective film [1]. Only exceptions were EDMed samples in oil bath herein only the samples machined at 500nF possessed slower $C.R._{corr}$ than non-machined samples. EDMed samples produced in oil bath at 10nF possessed higher $C.R._{corr}$ while that for the samples machined at 100nF, $C.R._{corr}$ was similar to non-EDMed sample $C.R._{corr}$. This means that the generation and thickness of the EDMed oxidised layer is encouraged with the increasing of the capacitance. These oxidised layer features define the corrosion rate of the samples. The capacitance used in EDM also had an influence on the corrosion rate ($C.R._{corr}$) of the samples fabricated in water and hydroxyapatite bath. For the samples machined in water, the $C.R._{corr}$ followed the order of 10nF > 500nF > 100nF. Lower capacitance values resulted in the formation of a thinner oxidised layer, while higher capacitance values led to the creation of cracks and imperfections that increased the susceptibility to corrosion [23]. On the other hand, for the samples produced in the hydroxyapatite dissolution bath, increasing the capacitance decreased the $C.R._{corr}$. This was attributed to the thicker hydroxyapatite layer formed on the surface at higher capacitance levels, as the capacitance promoted the deposition of hydroxyapatite on the Ti6Al4V material. The hydroxyapatite layer also exhibited a protective effect [1, 23]. It should be noted that the $C.R._{corr}$ of the EDMed samples could be lower due to the larger contact area between the aggressive environment and the metallic alloys caused by the higher average surface roughness [45].

The polarisation resistance (R_p) of the samples can be seen in **Fig.7(c)** and was estimated using the equation (2) [39, 46-48].

$$R_p = \frac{\beta_a * \beta_c}{2.303 * I_{corr} * (\beta_a + \beta_c)} \quad (2)$$

The anodic and cathodic slopes, denoted as β_a and β_c, respectively, exhibited contrasting trends compared to I_{corr} with respect to the electrical discharge machining parameters. This behaviour is expected since R_p (polarization resistance) and I_{corr} (corrosion current) are inversely proportional to each other [39, 46-48].

The passive film potential range (**Fig.7(d)**) was the substation of E_{tp} with E_{corr}. The samples machined in oil bath had lower passive film potential range than that for non-machined samples, indicating that the passive film of the samples machined in oil bath was less thermodynamic stable than the native passive film. Chang-bing et al. [32] noted that the titanium carbide formed during EDM process is less stable than pure oxide titanium layer for

SBF. The passive film range was reduced with the increment of the capacitance for the silicon oil bath. The cracks and the roughness decrease the stability of the passive film [45]. In the other bath, EDMed samples showed similar passive film potential range for each other and to non-EDMed samples.

The passive film corrosion rate was calculated using the equation (1), where I_{corr} was replaced by passive film current density that was defined how current density of the passive film potential range. Note that this is the predominant parameter in the corrosion kinetic for the passive materials. This parameter was dissimilar according to the EDM conditions (**Fig.7(d)**). The samples machined in the oil bath exhibited a higher corrosion rate of the passive film compared to the non-machined sample, indicating lower corrosion resistance. However, the sample machined at 100nF showed a similar corrosion rate to the non-EDMed samples, deviating from the trend. As previously explained, this can be attributed to the formation of a thin oxidised layer in the 10nF samples and the presence of a high number of imperfections in the 500nF samples. On the other hand, the samples machined in water and hydroxyapatite dissolution bath displayed a lower corrosion rate of the passive film compared to the non-machined samples. This can be attributed to the lower electrical conductivity of the passive film formed in the presence of water compared to the native passive film [11]. Furthermore, an increase in capacitance resulted in a reduction of the corrosion rate of the passive film in both cases. This can be attributed to the increased thickness of the passive film, which hinders electron transfer. Previous studies [26, 40] have also supported these findings.

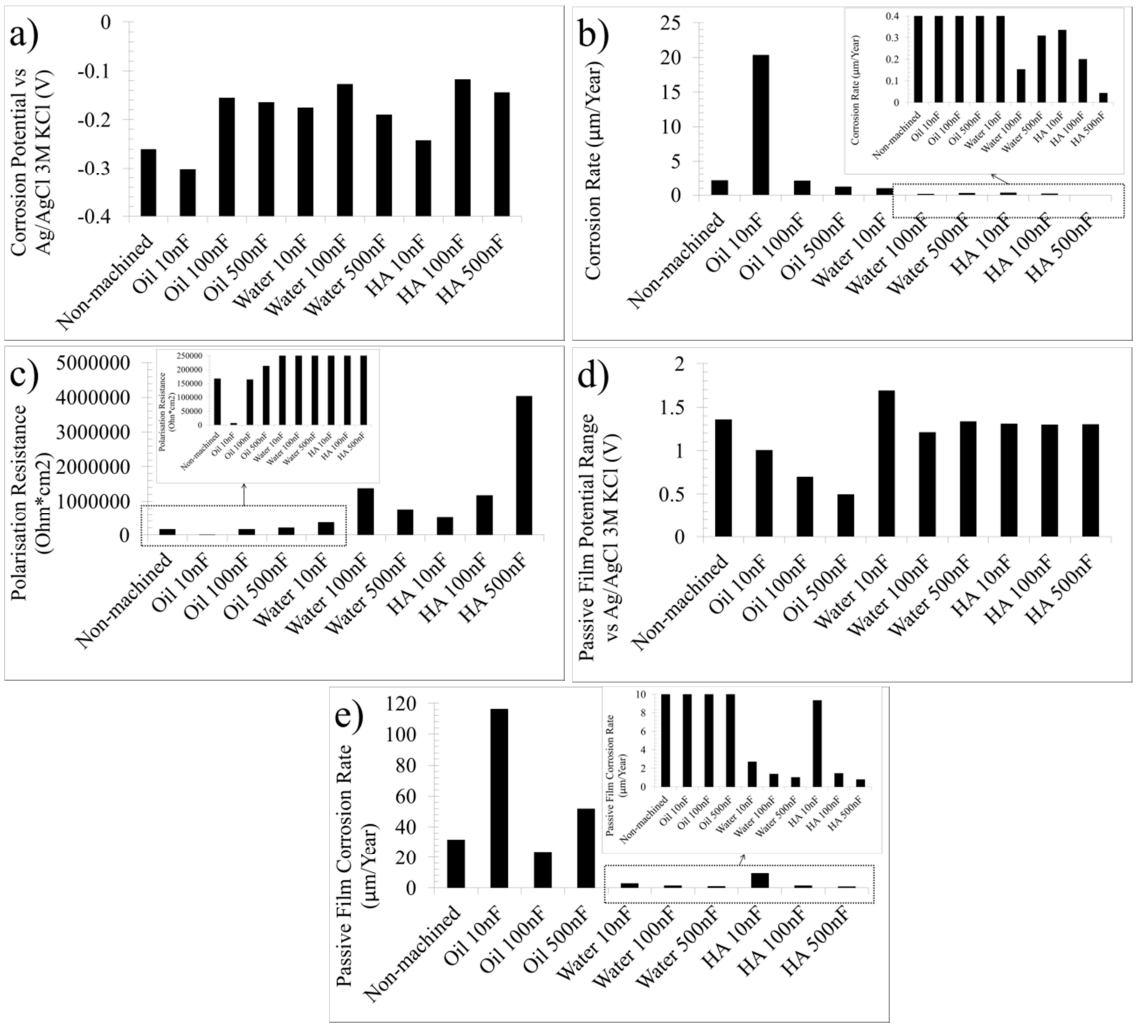

Figure 7. Graphs of the (a) corrosion potential, (b) corrosion current density, (c) polarisation resistance. (d) passivation potential range and (e) passivation film corrosion rate of the samples in SBF according to EDM conditions.

3.2.2. Electrochemical Impedance Spectroscopy, Alternating Current.

The EIS assessments of the non-machined and machined samples can be observed in **Fig. 8**. The equivalent circuit method, Bode and Nyquist plots were utilised to analyse the EIS data. EIS analyses showed that the samples had dissimilar corrosion mechanism. The non-EDMed sample before PPC exhibited a corrosion mechanism characterized by three distinct time constants. The first time constant was identified in the Bode plots, where the modulus impedance (Z_{mod}) showed a horizontal curve at high frequency (F) ranges (1000 Hz-100000 Hz), indicating the presence of a resistance component [49]. The second- and third-time constants were characterized by a rounded peak in the phase angle (θ) vs frequency (F) plots (Bode plots) at medium and low frequencies (0.01 Hz-1000 Hz). The distinct slopes of the inclined curves in the Z_{mod} vs F Bode plots also indicated the presence of these time constants. Both time constants showed a significant overlap, as evidenced by the rounded peak shape in the θ vs F Bode plots and the circular shape of the Nyquist plot [50]. These time constants were formed by a parallel combination of capacitance and resistance elements [50].

After the PPC, the non-machined sample exhibited a corrosion mechanism with a similar number and type of time constants, but the overlap between the second- and third-time constants was reduced. This can be observed in the significant difference in slopes of the

Bode plots (Z_{mod} vs F). The reduction in overlap suggests changes in the characteristics of the passive film [6, 13, 51].

The Bode and Nyquist plots of the samples machined in oil bath before PPC (**Fig.8(a)**) had similar the corrosion mechanisms than the non-machined samples. The visible double peaks of the Bode plots (Z_{mod} vs F) indicated the lower overlapping of second and third time constant. These signals were split in samples machined at higher capacity, meaning an increment of the microstructural change thickness with the increasing of the capacitance [52]. The overlapping of the second and third time constants was lower after PPC (**Fig. 8(b)**), showing a chemical change or degradation of the surface [6, 13, 51].

For the EDMed samples in a water bath before PPC (**Fig. 8(c)**), the corrosion mechanisms exhibited similar characteristics to the samples machined in an oil bath. The only difference was observed in the EDMed samples at 500nF, showing a shift towards lower frequencies after the PPC. This shift may indicate a decrease in corrosion resistance due to passive film degradation [4].

The samples machined in a hydroxyapatite dissolution bath (**Fig.8(d)**) before PPC also exhibited a similar corrosion mechanism to the previous samples. These machined samples showed a comparable overlapping of the second and third constants after PPC, indicating that the hydroxyapatite layer and passive film remained intact after the corrosion process [5, 50].

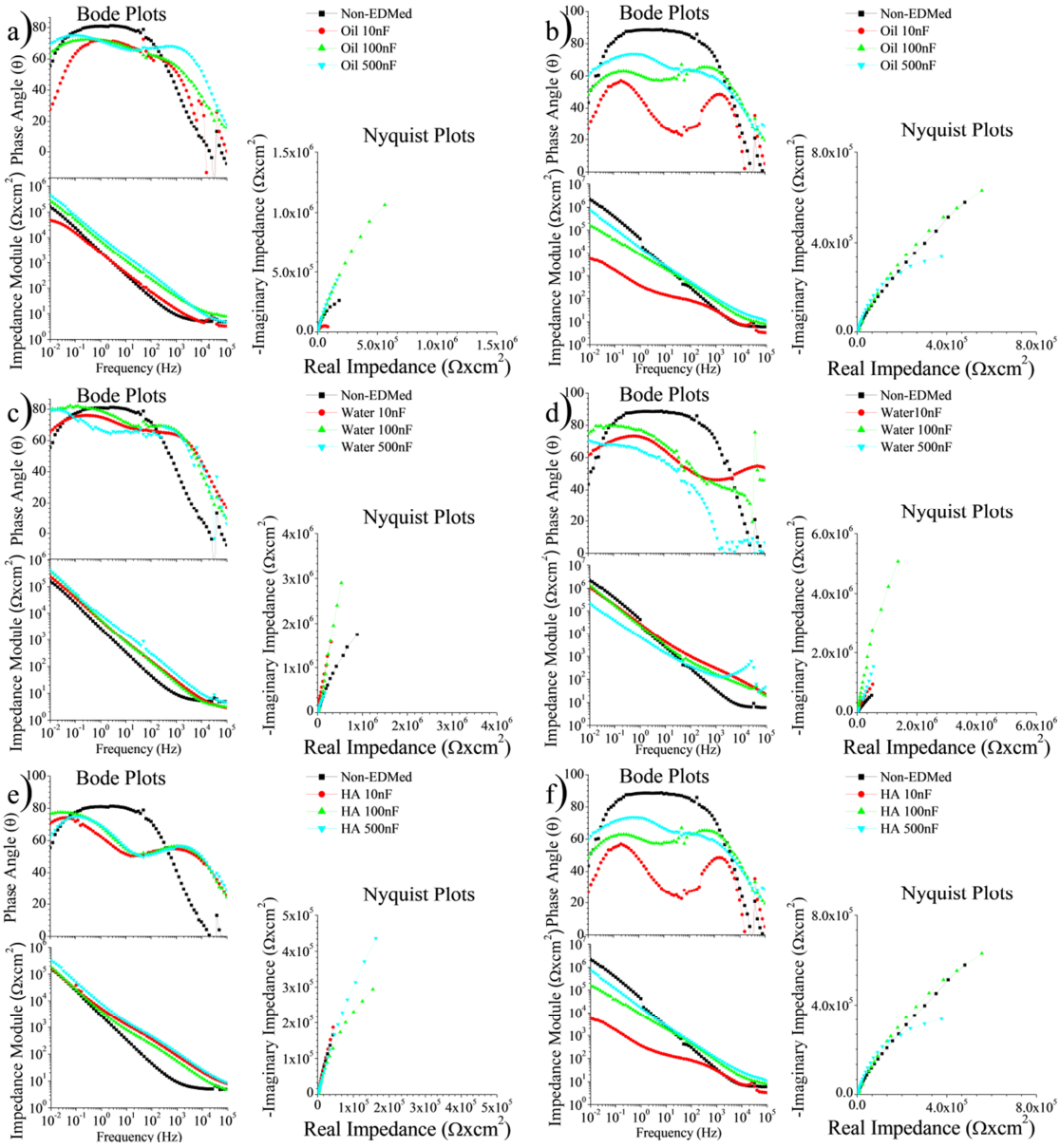

Figure 8. Bode and Nyquist plots illustrating the comparison between non-machined and machined Ti6Al4V samples in different environments: EDMed (a) and (b) represent oil, (c) and (d) represent water, and (e) and (f) represent a hydroxyapatite dissolution bath in simulated body fluid (SBF) before (a), (c), and (e) and after (b), (d), and (f) potentiostatic pulse current (PPC) treatment.

The values of the corrosion processes in the corrosion mechanisms were calculated using an equivalent circuit simulation, which represents the corrosion process using elements of an electrical circuit [19, 36, 38]. Three circuits were employed to represent the corrosion mechanism of the samples (**Fig. 9**), indicating that the initial assumption based on experimental data was incorrect. The first circuit (**Fig.9(a)**) closely resembled the proposed circuit based on experimental data. The first-time constant represented the dissolution resistance (R_s), and the second time constant represented the passive film (R_f and CPE_f). Both elements were in series with R_s. The final time constant corresponded to the charge transfer resistance (R_{ct}) and the charge double layer (CPE_{dl}) [5, 20, 50, 53]. The second equivalent circuit (**Fig. 9(b)**) was similar to the previous circuit, but R_f was absent. The last equivalent

circuit was identical to the previous circuit, except that CPE_f was replaced by bounded Warburg impedance (**Fig.9(c)**) [35].

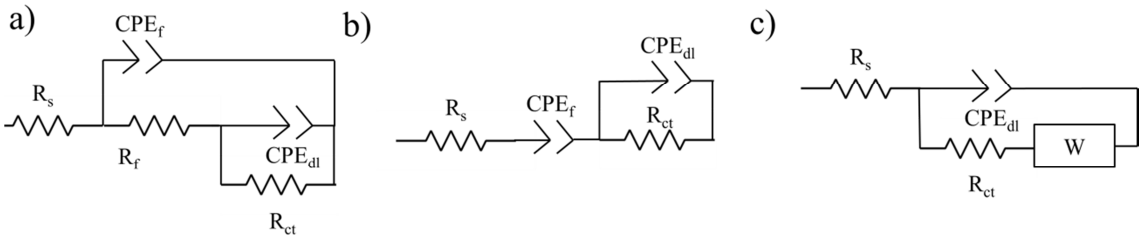

Figure 9. Schematic drawing of the (a) first, (b) second and (c) third equivalent circuit proposed.

The simulated data (**Fig. 10**) showed a good agreement with the experimental data, and the low chi-square values (**Table 4**), ranging from 10^{-4} to 10^{-3}, confirmed the validity of the simulation results [19]. The first equivalent circuit was the most observed circuit, representing most of the samples. The second circuit was found for the electrical discharge machined samples in water at 10nF before and after PPC, as well as in hydroxyapatite at 10nF before PPC. The third equivalent circuit represented the EDMed sample at 100nF in water and hydroxyapatite after PPC. The transpassivation process resulted in the formation of imperfections in the passive film, such as surface pitting and cracks, which influenced the diffusion processes within the film [36, 54].

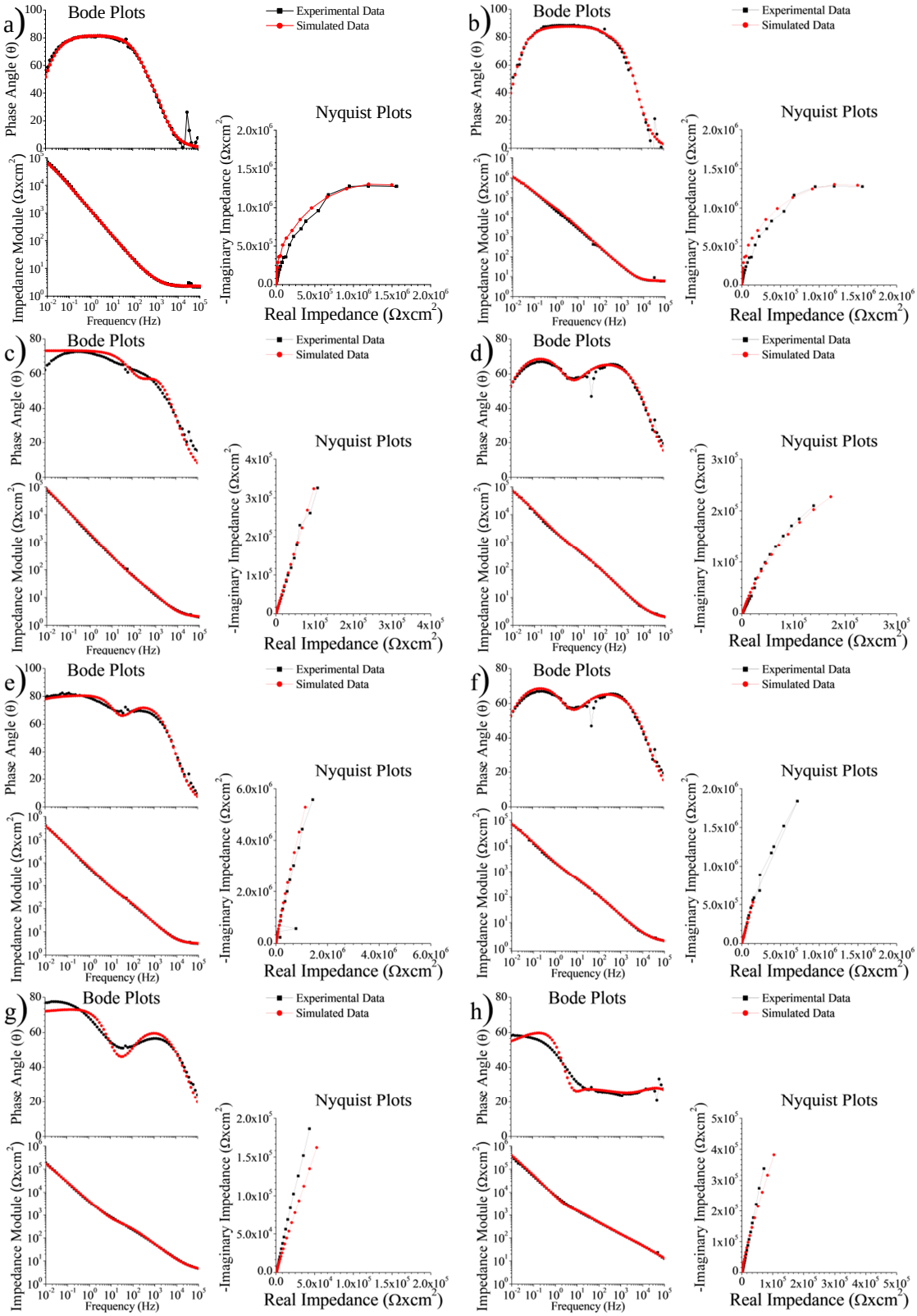

Figure 10. Comparison of the Bode and Nyquist plots between experimental and simulated data of the (a) and (b) non-machined and (c-h) machined at 10nF in oil c-d), water e-f) and hydroxyapatite dissolution g-h) bath for SBF immersion at 315K and 7.4pH.

Table 4 presents a summary of the values of the equivalent circuit elements. The values of R_S for all samples ranged from 2 Ω×cm^2 to 7 Ω×cm^2 indicating their dependency solely on the dissolution process [45, 49].

After PPC, there were notable changes in the other elements of the equivalent circuit. For the non-EDMed Ti6Al4V samples, R_f decreased while CPE_f increased, indicating that the protective capacity of the transpassivation passive film was lower compared to the original passive film. The value of n_f decreased from 1.00 to 0.90 after PPC, suggesting the presence of imperfections in the transpassivation film [4, 5, 20, 45]. On the contrary, R_{ct} increased after PPC, and CPE_{dl} decreased, indicating an improvement in the corrosion resistance of the exposed material. The value of n_{dl} remained at 0.85 after PPC, suggesting that the surface topography remained rough below the passive film [4, 5, 20, 45].

In contrast, the EDMed samples in the oil bath at 10nF and 100nF exhibited an opposite behaviour, indicating that the transpassivation process enhanced the corrosion resistance of the passive film. As for the EDMed samples in the HA dissolution bath, most of the equivalent circuit element values remained unchanged before and after PPC, indicating that the passive film formed in this process remained similar properties after transpassivation. After PPC treatment, the values of n_f and n_{dl} exhibited lower values, suggesting alterations in the material topography. However, these changes had minimal impact on the corrosion properties. Similar trends were observed for the EDMed samples in the water bath at 10nF, where R_{ct} increased, CPE_f and CPE_{dl} decreased after PPC, suggesting an increase in the chemical inactivity of the passive film. The values of n_f and n_{dl} remained similar before and after PPC. Similar evolution of the passive film was also observed in the EDMed samples in the oil and water baths at 500nF.

Table 4. The equivalent circuit element values for the non-machined and EDMed Ti6Al4V

Sample	PPC	R_s (Ωxcm^2)	R_f ($k\Omega xcm^2$)	CPE_f ($\mu S/sxcm^2$)	n_f	R_{ct} ($k\Omega xcm^2$)	CPE_{dl} ($\mu S/sxcm^2$)	n_d	W ($\mu S/s^{1/2}xcm^2$)	n_W	X^2 (10^{-3})
Non-machined	Before	6.131	2610.000	5.258	1.00	0.150	6106.782	0.85	-	-	0.987
	After	1.96	0.599	253.798	0.9	9510.000	9.510	0.85	-	-	1.043
Oil 10nF	Before	4.021	0.159	37.210	0.87	117.716	26.362	0.93	-	-	0.525
	After	5.017	249.788	40.298	0.76	15.893	133.690	0.93	-	-	0.374
Oil 100nF	Before	7.802	0.307	18.500	0.80	1540.000	96.200	0.84	-	-	1.640
	After	6.866	6.040	16.500	0.76	846.000	10.400	0.86	-	-	1.480
Oil 500nF	Before	2.820	16.1710	63.948	0.75	20.401	130.252	0.82	-	-	1.570
	After	2.099	0.364	132.385	0.70	43.134	1.581	1.00	-	-	5.860
Water 10nF	Before	4.711	-	10.050	0.81	3.080	11.110	0.76	-	-	1.430
	After	6.486	-	4.740	0.82	0.618	3.703	0.72	-	-	0.701
Water 100nF	Before	2.919	0.240	111.748	0.76	2140.000	33.062	0.90	-	-	0.563
	After	3.778	-	-	-	0.011	124.078	0.80	45.900	0.98	0.563
Water 500nF	Before	5.180	1.563	8.277	0.89	1720.000	6.338	1.00	-	-	0.564
	After	3.905	0.265	12.621	0.80	1180.000	6.028	0.86	-	-	0.563
HA 10nF	Before	4.712	-	11.110	0.76	2.177	10.500	0.81	-	-	1.430
	After	2.960	0.589	250.580	0.50	9508.000	51.334	0.82	-	-	1.420
HA 100nF	Before	3.819	0.757	28.351	0.74	19014.534	27.035	0.90	-	-	1.920
	After	2.424	-	-	-	0.086	8.979	0.68	60.719	0.32	2.710
HA 500nF	Before	6.240	1.480	15.800	0.72	4530.973	12.000	0.89	-	-	4.370
	After	7.100	1.927	14.012	0.59	2312.139	21.221	0.79	-	-	1.360

3.3. Microstructure analysis after electrochemical test

The surface characteristics of the samples before and after PPC are shown in **Fig. 11**. The surfaces of the EDMed samples exhibited a similar appearance, indicating that the transpassivation process had only a minor effect on the surface topography. In contrast, the non-EDMed samples showed a darkened area after PPC, indicating the oxidation of the Ti6Al4V material. The occurrence of localized oxidations can be attributed to the transpassivation process [12, 38]. However, in the case of the EDMed samples, such darkened areas were not observed because the material had already undergone oxidation during the EDM process [25, 26].

After PPC, the cross-section of the EDMed samples exhibited an additional layer, being attributed to the deposition of dissolved salts. During the PPC process, a portion of the electrical current can be utilized to transfer ions, which are subsequently reduced and deposited onto the surface [38]. This deposited layer displayed a higher prevalence of cracks and pores. It is noteworthy that all samples exhibited cracks both before and after PPC, indicating that the transpassivation process did not significantly alter the internal structure of the Ti6Al4V material.

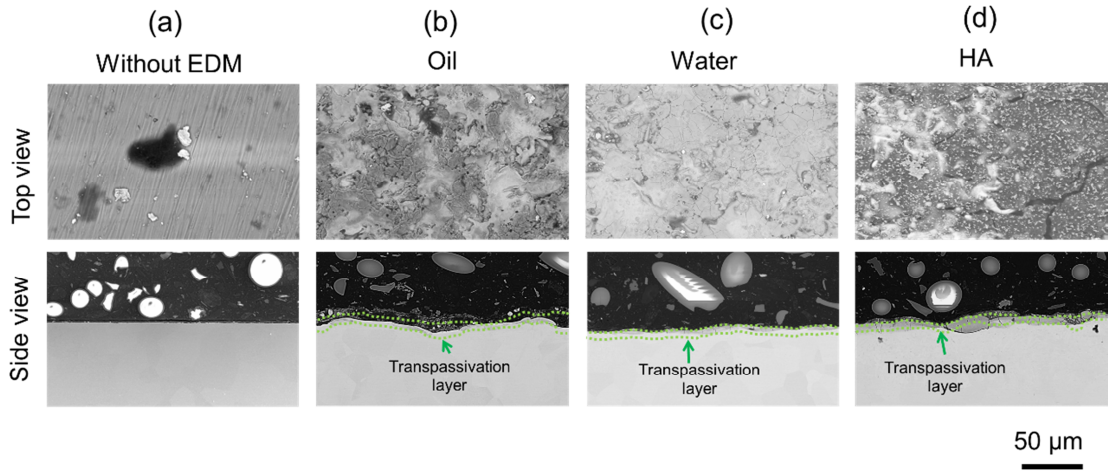

Figure 11. SEM micrograph of (a) non-EDMed (without EDMed) and samples EDMed (100nF) samples at (b) oil, (c) water and (d) HA bath (after PPC study).

The chemical composition maps of the sample cross sections focused on interested elements (titanium, oxygen and carbon) can be seen in **Fig. 12**. Non-EDMed specimens were mainly formed of titanium, indicating the passive film of this sample is thin. Oil bath samples had a low titanium concentration on the surface and localised zones with high oxygen and carbon concentration. Although the carbon was present on the surface, the concentration was dissimilar on the surface. These outcomes indicated that the surface chemical composition of these specimens was heterogeneous, which is a cause of their low corrosion resistance. Holsten et [55] observed that this is due to the cathodic (negative) polarisation of the tool hinders the carbon reaction with the Ti6Al4V and pure-Ti in oil bath. This causes a heterogeneous and thin titanium carbide layer. The researchers also observed that the samples EDMed in water bath had surface totally oxidised, indicating that this process only occur in oil bath. EDMed samples in

water and HA bath showed a high oxygen concentration on surface and low titanium concentration. The presence of a thick passive film on these specimens has been revealed by these results, indicating its formation during the EDM process, as previously mentioned. EDMed samples in water bath possessed a passive film thicker than the surface generated in HA dissolution in distilled water, which is a reason of the better corrosion resistance of the water EDMed specimens as described before. In both cases, the passive film was larger than non-EDMed specimens, providing their superior corrosion resistance.

Notting EDS is infeasible to determine the chemical compound with exactitude because this technique can only detect the elements and not the molecules. TiO_2 and TiC however are the most common molecules when the oxygen concentration is high. On other hand, the non-stoichiometric molecules (TiO_X and Ti_XC) are the most usual for low oxygen concentration. Aluminium and vanadium oxidise can be found these zones.

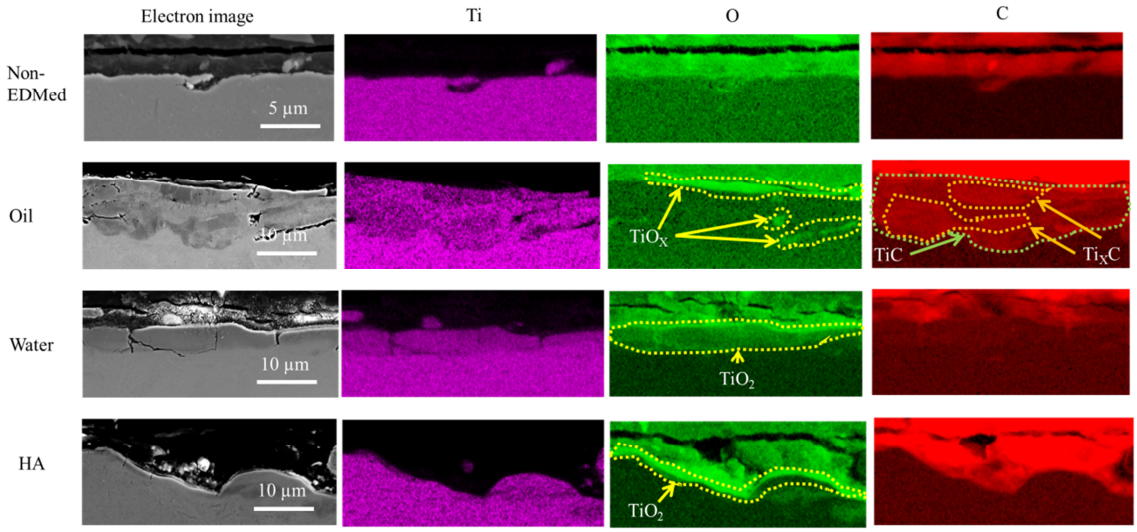

Figure 12. EDS chemical composition maps of the 10nF samples after PPC study where TiO_X is non-stoichiometric titanium oxide with oxygen deficient, TiO_2 is titanium dioxide, TiC_X is non-stoichiometric titanium carbide with carbon deficient and TiC is titanium carbide.

4 Discussion

The dissimilarity in corrosion resistance among the samples is attributed to the formation of an oxide layer during EDM. Samples subjected to a less aggressive environment, such as an oil bath and low capacitance, exhibited a heterogeneous and thin oxidised layer. The charge transfer of the passive film was inversely proportional to the thickness of the passive film [25, 26], resulting in an anodic effect on the non-oxidised areas, thereby promoting corrosion [7]. Increasing the capacitance (500nF) mitigated this effect; however, it led to the formation of cracks and a higher average roughness, which consequently decreased corrosion resistance. The roughness contributed to an increase in the exposed area and the presence of crevices [45], while

cracks further facilitated crevice corrosion [2]. Consequently, EDMed samples produced in an oil bath demonstrated lower corrosion resistance compared to non-EDMed samples.

The adverse effects of cracks and roughness on the corrosion surface were eliminated when the oxidised layer became homogeneous and thick. This condition was achieved in aggressive environments such as water and hydroxyapatite dissolution, coupled with high capacitance. The environment supplied oxidant elements that chemically activated the metallic alloy [15, 25] in conjunction with the capacitance [52]. The presence of the oxidised layer even eliminated the detrimental effects of cracks, being typically caused by thermal stress [2]. As a result, EDMed samples fabricated in water and hydroxyapatite demonstrated higher corrosion resistance compared to non-EDMed samples. It is worth noting that hydroxyapatite EDMed samples exhibited lower corrosion resistance than water EDMed samples. The potential part of PPC, represented by the anodic branch passivation range, was utilized for depositing SBF ions onto the Ti6Al4V surface [38, 40]. The thickness of the oxidised layer can chemically be inactivated and is directly proportional to the EDM capacitance [26, 40]. While the hydroxyapatite coating provides a protective effect, it is relatively weaker compared to the protection offered by the oxidised layer. The highest corrosion resistance was observed in EDMed samples produced at the highest capacitance, owing to the dependence of the corrosion resistance with the oxidised layer thickness.

The corrosion mechanisms observed in the Ti6Al4V samples were generally similar across all samples. These mechanisms consisted of a solution resistance, a passive film, and exposed materials. The passive film surfaces of the EDMed samples exhibited roughness, resulting in a surface roughness factor (n_f) lower than 1, primarily due to the generation of pores on the outer layer [4, 5, 20, 45]. The presence of these similar corrosion mechanisms indicated that the presence of cracks and high average roughness had a minimal effect on the corrosion behaviour of EDMed Ti6Al4V, as the samples exhibited significant corrosion resistance.

The impact of transpassivation on corrosion resistance (as observed through EIS) varied among the samples. The microstructures of the samples remained unchanged after PPC. Transpassivation induced a chemical evolution of the passive film, leading to modifications in its chemical structure. This chemical evolution could differ based on the elements involved in the formation of the passive film, which in turn depended on the EDM parameters [36]. Notably, the influence of transpassivation on the corrosion resistance of samples immersed in a HA dissolution in distilled water bath was minimal, indicating the high stability of the passive film in this case [1, 50]. The additional layer formed during PPC through the electrodeposition of SBF salt had a negligible effect on corrosion resistance. The presence of a high number of defects, such as cracks and pores, in the deposited layer significantly reduced its protective capabilities [23].

5 Conclusions

Based on a comprehensive electrochemical and microstructural study, the corrosion characteristics of the Ti6Al4V alloy were investigated under different EDM conditions in simulated body fluid. The following conclusions can be drawn from this analysis:

The EDMed samples exhibited higher nobility compared to the non-EDMed samples, primarily attributed to the formation of an oxidised layer during the electrical discharge machining processes.

The corrosion resistance of samples machined using electrical discharge in aggressive baths (such as water and hydroxyapatite dissolution) is higher compared to non-EDMed samples. When EDM is performed in an oil bath, the corrosion resistance of the samples decreases due to the formation of a heterogeneous layer. Samples furthermore produced with high capacitance exhibit greater corrosion resistance than those EDMed at low capacitance.

The corrosion mechanism remains similar for all samples before PPC, but it diverges afterward. The chemical evolution resulting from transpassivation varies depending on the oxidised elements present in the passive film. Additionally, this process leads to the electrodeposition of SBF elements on Ti6Al4V samples.

Although EDM samples immersed in water exhibit the highest corrosion resistance, an additional beneficial property is the presence of a hydroxyapatite film on these samples, which contributes to good biointegrity.

This research provides a cost-effective and efficient method for generating Ti6Al4V surfaces that offer both high corrosion resistance and excellent biointegration. The implications of this work are significant, benefiting various industries, particularly the biomedical sector.

Declaration of Competing Interest

The authors have no conflicts of interest.

Acknowledgement

This work was partially supported by Liverpool John Moore University, Faculty of Engineering and Technology (FET) Pump Prime Awards 2021/22.

References

[1] P.S. Bains, M. Bahraminasab, S.S. Sidhu, G. Singh, Proceedings of the Institution of Mechanical Engineers, Part H: Journal of Engineering in Medicine, 234 (2020) 232-242.

[2] G. Singh, T.R. Ablyaz, E.S. Shlykov, K.R. Muratov, A.S. Bhui, S.S. Sidhu, Micromachines, 11 (2020) 850.

[3] I. Lavos-Valereto, S. Wolynec, I. Ramires, A.C. Guastaldi, I. Costa, Journal of Materials Science: Materials in Medicine, 15 (2004) 55-59.

[4] V. Alves, R. Reis, I. Santos, D. Souza, T.d.F. Gonçalves, M. Pereira-da-Silva, A. Rossi, L. Da Silva, Corrosion Science, 51 (2009) 2473-2482.

[5] M. Hussein, A. Madhan Kumar, A.F. Abdelaal, M. Abdul Azeem, Metallurgical and Materials Transactions A, 52 (2021) 4299-4309.
[6] S. Tamilselvi, V. Raman, N. Rajendran, Electrochimica Acta, 52 (2006) 839-846.
[7] B. Sivakumar, S. Kumar, T.S. Narayanan, Wear, 270 (2011) 317-324.
[8] C.A.R. Maestro, M.C. Ferreira, A.H.S. Bueno, A.M. de Sousa Malafaia, Engineering Journal, 24 (2020) 185-193.
[9] R.W.-W. Hsu, C.-C. Yang, C.-A. Huang, Y.-S. Chen, Materials Science and Engineering: A, 380 (2004) 100-109.
[10] R. Luo, Z. Liu, F. Yan, Y. Kong, Y. Zhang, Applied surface science, 266 (2013) 57-61.
[11] J. Lu, G. Wei, Y. Yu, X. Zhao, Y. Dai, Int J Electrochem Sci, 12 (2017) 2763-2776.
[12] H.R.A. Bidhendi, M. Pouranvari, Metallurgical and Materials Engineering, (2012).
[13] E. Matykina, R. Arrabal, B. Mingo, M. Mohedano, A. Pardo, M. Merino, Surface and Coatings Technology, 307 (2016) 1255-1264.
[14] C. Prakash, M. Uddin, Surface and Coatings Technology, 326 (2017) 134-145.
[15] M. Al-Amin, A.M. Abdul-Rani, M. Danish, S. Rubaiee, A.b. Mahfouz, H.M. Thompson, S. Ali, D.R. Unune, M.H. Sulaiman, Materials, 14 (2021) 3597.
[16] A. Mahajan, S. Devgan, S.S. Sidhu, Surface and Coatings Technology, 405 (2021) 126583.
[17] S.K. Manderna, P. Katyal, M. Gupta, V. Singh, in: IOP Conference Series: Materials Science and Engineering, IOP Publishing, 2022, pp. 012067.
[18] D. Krupa, J. Baszkiewicz, B. Rajchel, A. Barcz, J. Sobczak, A. Biliński, T. Borowski, Vacuum, 81 (2007) 1310-1313.
[19] A.A. El Hadad, E. Peón, F.R. García-Galván, V. Barranco, J. Parra, A. Jiménez-Morales, J.C. Galván, Materials, 10 (2017) 94.
[20] X. Chen, Q. Liao, M. Gong, Q. Fu, Metals, 13 (2023) 192.
[21] M.A. Hussein, N. Ankah, A.M. Kumar, M.A. Azeem, S. Saravanan, A.A. Sorour, N. Al Aqeeli, Ceramics International, 46 (2020) 18573-18583.
[22] M. Kalisz, M. Grobelny, M. Zdrojek, M. Świniarski, J. Judek, Thin Solid Films, 596 (2015) 101-110.
[23] H. Yaşar, B. Ekmekci, Surface Topography: Metrology and Properties, 9 (2021) 015015.
[24] S. Sethy, R.K. Behera, J.P. Davim, J. Rana, Journal of Manufacturing and Materials Processing, 6 (2022) 96.
[25] A. Pramanik, A. Basak, G. Littlefair, S. Debnath, C. Prakash, M.A. Singh, D. Marla, R.K. Singh, Heliyon, 6 (2020) e05554.
[26] J.T. Philip, J. Mathew, B. Kuriachen, Journal of Manufacturing Processes, 64 (2021) 1105-1142.
[27] N. Ekmekci, B. Ekmekci, Materials and Manufacturing Processes, 31 (2016) 1663-1670.
[28] O. Tahsin, H. Yasar, M. MURPHY, N. EKMEKCİ, B. EKMEKCİ, International Journal of Advances in Engineering and Pure Sciences, 31 (2018) 1-10.
[29] S.-L. Chen, M.-H. Lin, G.-X. Huang, C.-C. Wang, Applied surface science, 311 (2014) 47-53.
[30] P. Harcuba, L. Bačáková, J. Stráský, M. Bačáková, K. Novotna, M. Janeček, Journal of the mechanical behavior of biomedical materials, 7 (2012) 96-105.
[31] F. Otsuka, Y. Kataoka, T. Miyazaki, Dental materials journal, 31 (2012) 309-315.
[32] T. Chang-bin, L. Dao-Xin, W. Zhan, G. Yang, Applied surface science, 257 (2011) 6364-6371.

[33] Y. Sasikumar, M. Solomon, L. Olasunkanmi, E. Ebenso, Materials and Corrosion, 68 (2017) 776-790.
[34] S. Esmailzadeh, M. Aliofkhazraei, H. Sarlak, Protection of metals and physical chemistry of surfaces, 54 (2018) 976-989.
[35] J.I. Ahuir-Torres, J. Hernández-López, M. Arenas, A. Conde, J. De Damborenea, Surface and Coatings Technology, 259 (2014) 408-414.
[36] G. Yi, X. Liu, C. Zheng, H. Zhang, C. Xu, Y.-W. Cui, S. Liu, Frontiers in Materials, 7 (2021) 640081.
[37] Q. Zhang, B. Duan, Z. Zhang, J. Wang, C. Si, Journal of Materials Research and Technology, 11 (2021) 1090-1099.
[38] S.L. de Assis, S. Wolynec, I. Costa, Electrochimica Acta, 51 (2006) 1815-1819.
[39] R.G. Kelly, J.R. Scully, D. Shoesmith, R.G. Buchheit, Electrochemical techniques in corrosion science and engineering, CRC Press, 2002.
[40] L.-Y. Chen, H.-Y. Zhang, C. Zheng, H.-Y. Yang, P. Qin, C. Zhao, S. Lu, S.-X. Liang, L. Chai, L.-C. Zhang, Materials & Design, 208 (2021) 109907.
[41] F. Endres, S.Z. El Abedin, A. Saad, E. Moustafa, N. Borissenko, W.E. Price, G.G. Wallace, D.R. Macfarlane, P.J. Newman, A. Bund, Physical Chemistry Chemical Physics, 10 (2008) 2189-2199.
[42] A. Schmon, K. Aziz, G. Pottlacher, in: EPJ Web of Conferences, EDP Sciences, 2017, pp. 04003.
[43] V. Bower, R. Davis, T. Murphy, P. Paulsen, J. Gramlich, L. Powell, JOURNAL OF RESEARCH of the National Bureau of Standards, 87 (1982) 21.
[44] F. Mansfeld, Corrosion, 29 (1973) 397-402.
[45] A. Toloei, V. Stoilov, D. Northwood, in: ASME International mechanical engineering congress and exposition, American Society of Mechanical Engineers, 2013, pp. V02BT02A054.
[46] G. Kear, F.C. Walsh, Corrosion and materials, 30 (2005) 51-55.
[47] X. Zhang, Z.H. Jiang, Z.P. Yao, Y. Song, Z.D. Wu, Corrosion Science, 51 (2009) 581-587.
[48] K. Kakaei, M.D. Esrafili, A. Ehsani, Graphene and anticorrosive properties, in: Interface science and technology, Elsevier, 2019, pp. 303-337.
[49] E. McCafferty, Introduction to corrosion science, Springer Science & Business Media, 2010.
[50] K. Leksycki, A. Kaczmarek-Pawelska, K. Ochał, A. Gradzik, D.Y. Pimenov, K. Giasin, D. Chuchala, S. Wojciechowski, Materials, 14 (2021) 6917.
[51] I.-J. Hwang, H.-C. Choe, W.A. Brantley, Surface and Coatings Technology, 320 (2017) 458-466.
[52] M.V. Diamanti, F. Bolzoni, M. Ormellese, E. Pérez-Rosales, M. Pedeferri, Corrosion engineering, science and technology, 45 (2010) 428-434.
[53] A. Lasia, Electrochemical impedance spectroscopy and its applications, Springer, 2002.
[54] J.C. Grotberg, in, University of Illinois at Chicago, 2014.
[55] M. Holsten, P. Koshy, A. Klink, A. Schwedt, CIRP Annals, 67 (2018) 221-224.